HOSTED BY
ELSEVIER
Available online at www.sciencedirect.com
ScienceDirect
Soils and Foundations 64 (2024) 101466
SOILS AND FOUNDATIONS
www.elsevier.com/locate/sandf

Technical Paper

Experimental study of factors affecting the viscosity-based pore pressure generation model and the pseudo plastic behaviour of liquefiable soils

Lucia Mele [a,*], Stefania Lirer [b], Alessandro Flora [a]

[a] University of Napoli Federico II, Italy
[b] University of Roma Guglielmo Marconi, Italy

Received 13 September 2023; received in revised form 9 March 2024; accepted 8 April 2024

Abstract

Fully liquefied soils behave like viscous fluids, and models developed within the framework of soil mechanics fail to catch their behaviour on the verge of liquefaction or after it. Several research works have shown that modelling the liquefied soil as a fluid is physically more convincing. Such an equivalent fluid can be characterised via an apparent viscosity (η) (sharply dropping when liquefaction is triggered) which can be modelled as a power law function of the shear strain rate (pseudo-plastic fluid), depending on two parameters: the *fluid consistency coefficient* (*k*) and the *liquidity index* (*n*). With this approach, it is possible to consider a simple correlation between the equivalent viscosity and pore pressure increments independent on the equivalent number of cycles, whose parameters can be calibrated from the results of stress-controlled laboratory tests. The paper investigates the effect of some relevant experimental factors (effective vertical stress, stress path, frequency and waveform of the applied cyclic load, soil fabric and pre-existing shear stress) on the apparent viscosity of soils during their transition from the solid to the liquefied state, and therefore also on the pore pressure increments generated by the stress path. To do that, the results of stress-controlled laboratory tests performed in a sophisticated simple shear apparatus, along with published data, have been interpreted in terms of the apparent viscosity. Simple correlations in terms of viscosity-based pore pressure generation and pseudo-plastic behaviour are proposed and confirmed from the results of 1D non-linear site response analysis for the case study of Scortichino (Italy).

Keywords: Apparent viscosity; Simple shear tests; Viscosity-based excess pore water pressure generation model; Pseudo-plastic behaviour; Liquefied soils

1. Introduction

As reported by the Committee on Soil Dynamics of the Geotechnical Engineering Division (1978) of the American Society of Civil Engineers, the term "liquefaction" is generally used to describe "*the act or process of transformation of any substance into a liquid*". Generally, loose, saturated sandy soils can be prone to liquefaction phenomenon if subjected to rapid loading paths, such as earthquakes. It is due to the fact that they are not able to quickly dissipate the earthquake induced excess pore water pressure (Δu). The sudden increase of pore water pressure results in a reduction of the effective stresses until approaching zero. Under this condition a change of soil state from solid to liquid occurs, leading to catastrophic consequences on built environment (Tokimatsu & Asada, 1998; Cubrinovski et al., 2011; Vannucchi et al., 2012; Towata et al., 2014; Baris et al., 2021; Castiglia et al., 2021) as happened recently in 2023-earthquake sequence in Turkey.

Since liquefied soils behave like fluid more than solid, they should be modelled using fluid mechanic models

* Corresponding author.
E-mail address: lucia.mele@unina.it (L. Mele).

https://doi.org/10.1016/j.sandf.2024.101466

Notation list

CRR	cyclic resistance ratio
CSR	cyclic stress ratio
Dr	relative density
D_{50}	average diameter
e_{max}	maximum void ratio
e_{min}	minimum void ratio
f	frequency
FC	fines content
k	fluid consistency coefficient
n	liquidity index
N_{cyc}	number of cycles
N_{liq}	number of cycles at liquefaction
r_u	excess pore pressure ratio
U_c	uniformity coefficient
z	depth
α	static shear stress ratio
γ	shear strain
$\dot{\gamma}$	shear strain rate
η	apparent viscosity
η_0	initial apparent viscosity
η_{fluid}	apparent viscosity in fluid phase
σ'_{v0}	initial effective vertical stress
σ'_v	effective vertical stress
σ'_{h0}	initial effective horizontal stress
σ'_h	effective horizontal stress
τ	shear stress
τ_{cyc}	cyclic shear stress
τ_s	static shear stress

(Sasaki et al., 1992; Miyajima et al., 1995; Schenkengel & Vrettos, 2014). Uzuoka et al. (1998), Chen et al., (2006; 2011) and more recently Chiou & Ng (2022), proposed to describe liquefied soils as non-Newtonian fluids, developing a numerical analysis method to investigate the behavior of the lateral flow of liquefied soils. Lu et al., (2023a-b) estimated the liquefaction-induced settlements of shallow foundations and the uplift of manholes in liquefied soils by modelling soil as fluid.

On the other hand, Towhata et al. (1999) observed that liquefied sands exhibited properties typical of pseudo-plastic non-Newtonian fluids. Congruently Hamada and Wakamatsu (1998) proposed to study the behaviour of liquefied soils as a pseudo-plastic fluid through the following equation:

$$\eta = \frac{\tau}{\dot{\gamma}} = k \cdot (\dot{\gamma})^{(n-1)} \quad (1)$$

where τ is shear stress, $\dot{\gamma}$ is the shear strain rate, η is the viscosity of the fluid and k and n are the *fluid consistency coefficient* and *liquidity index*, respectively (Zhou et al., 2014). Obviously, the two parameters *k* and *n* depend on the kind of fluid. As reported by Zhou et al. (2014) k can reflect the consistency of fluid while n can reflect the nature of the fluid. A Newtonian fluid has $n = 1$, while non-Newtonian fluids exhibit $n \neq 1$, in particular, when $n < 1$, the fluid is *shear thinning flow*, when $n > 1$, the fluid is a *shear thickening flow* (Fig. 1).

Therefore, the stress–strain response of a liquefiable soil undergoing cyclic loads (i) can be processed in the framework of fluids mechanic, computing an "*apparent viscosity*" defined (Chen et al., 2016) in each loading cycle of undrained tests (η_i) as:

$$\eta_i = \frac{\tau_{i,max} - \tau_{i,min}}{\dot{\gamma}_{i,max} - \dot{\gamma}_{i,min}} \quad (2)$$

where $\tau_{i,max}$ and $\tau_{i,min}$ are the maximum and minimum values of the applied cyclic shear stress and $\dot{\gamma}_{i,max}$ and $\dot{\gamma}_{i,min}$ are the shear strain rates. It is worth noting that Eq. (2) can be used in stress-controlled tests. On the contrary, it cannot be applied in strain-controlled tests. However, it should be emphasized that stress-controlled tests are able to better simulate what happens in situ when a seismic event occurs, while strain-controlled tests are generally preferred to evaluate the cyclic (or dynamic) properties of soils.

Mele (2022), by processing more than 40 cyclic undrained triaxial tests carried out on 6 different sandy soils ($0 < FC < 11$ %; $0.1 < D_{50} < 0.5$ mm; $1 < U_c < 5$) in different conditions ($25 < D_r < 68$ %; $25 \leq \sigma'_c \leq 100$ kPa; $f = 0.008$ Hz), confirms that the values of η (Eq. (2)) decrease with increasing $\dot{\gamma}$ (Fig. 2a) according to the correlation expressed by Eq. (1). Furthermore, as shown in Fig. 2b, the fluid consistency coefficient (k) seems to be dependent on the applied cyclic stress ratio CSR (defined as the ratio between the cyclic shear stress τ_{cyc} and the effective vertical stress σ'_{v0}) and the liquidity index (n) is always less than 1 (*shear thinning flow*, Fig. 1) and mainly affected by k (Fig. 2c).

The potential of the apparent viscosity in the study of the cyclic response of liquefiable sandy soils during undrained loading condition has already been highlighted by Lirer & Mele (2019) and Mele (2022). In Fig. 3a, the expected trend of the apparent viscosity decay law with the number of loading cycles (N_{cyc}) has been reported. For loading cycles far from liquefaction triggering, the soil is in a solid phase with values of η almost constant and quite close to the initial one η_0 ($N_{cyc} = 0$): after that, the loading path moves into a transition zone in which the two phases (solid and liquid) coexist and the apparent viscosity suddenly decreases. When liquefaction starts to develop, the soil becomes a liquid and a minimum single value of apparent viscosity should be expected (η_{fluid}). As

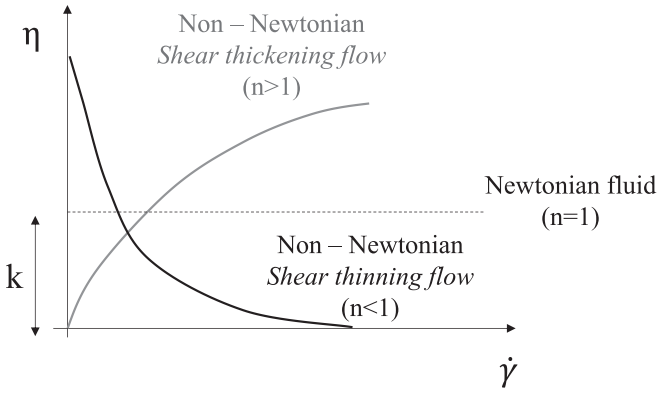

Fig. 1. Rheological behaviour of a fluid in strain rate ($\dot{\gamma}$)- viscosity (η) plane.

reported by Lirer & Mele (2019), liquefaction is attained in correspondence with the elbow of the $\eta - N_{cyc}$ decay law. For saturated sandy soils, in correspondence with the elbow of the viscosity curve, r_u generally assumes a value equal to 0.90 (Fig. 3b), where r_u is the pore pressure ratio ($\Delta u/\sigma'_{v0}$), the stress parameter traditionally adopted to identify the liquefaction triggering in silty sands (Ishihara, 1993). It can be assumed that liquefaction starts to develop when excess pore water pressure is 90 % of the effective vertical stress. On the contrary, for $r_u = 1.0$, full liquefaction is attained. Considering $r_u = 0.90$ is a conservative way to identify the onset of liquefaction.

Lirer & Mele (2019), analyzing the results of cyclic undrained triaxial tests carried out on reconstituted and undisturbed (frozen) specimens of sandy and gravelly soils in terms of apparent viscosity decay law, highlighted the strong link between η and r_u, introducing a viscosity-based excess pore water pressure generation model represented by the following relationship:

$$\frac{\eta}{\eta_0} = \frac{1 - r_u^a}{1 + b \cdot r_u^c} \tag{3}$$

where a, b and c are soil parameters that should be calibrated on the experimental results.

Eq. (3) has been further validated by Mele (2022). As an example, in Fig. 3c the experimental data of Ticino sand (FC = 0 %) have been plotted in the plane $r_u - \eta/\eta_0$ together with the approximate relationship expressed by Eq. (3). It is worth emphasizing that the parameters of Eq. (3) do not depend on CSR or N_{liq}, therefore, contrary to the traditional stress and strain-based pore pressure generation models (i.e., Booker et al., 1976; Dobry et al., 1985), this pore water generation model does not need a complex conversion in equivalent number of cycles, like the innovative energy-based pore generation models (i.e., Berrill & Davis, 1985; Green et al., 2000).

Eq. (3) has been obtained only through cyclic triaxial tests, therefore it could be useful to validate it by performing cyclic simple shear tests that more correctly reproduce within the soil the stress path experienced by soils during real earthquakes. To this aim, a wide experimental study

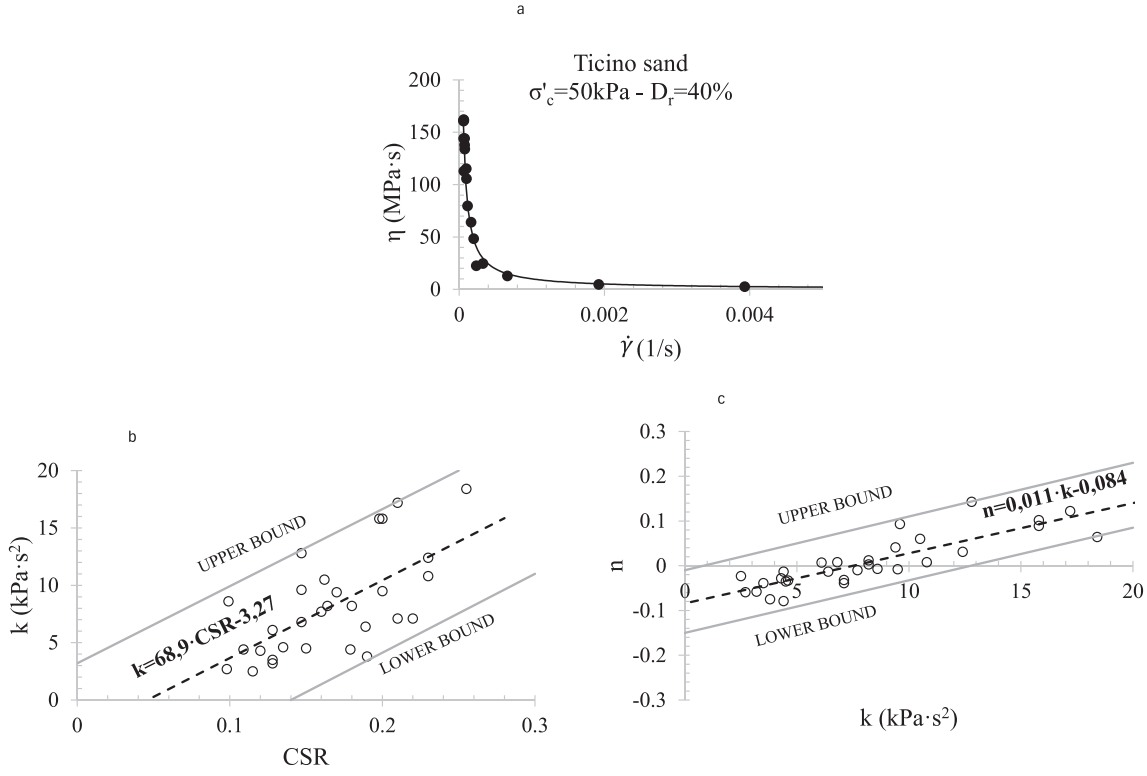

Fig. 2. Example of pseudo-plastic behaviour of sandy soil (a) and fluid consistency coefficient (k) versus CSR (b) and linear relationship between k and n (c) (after Mele, 2022).

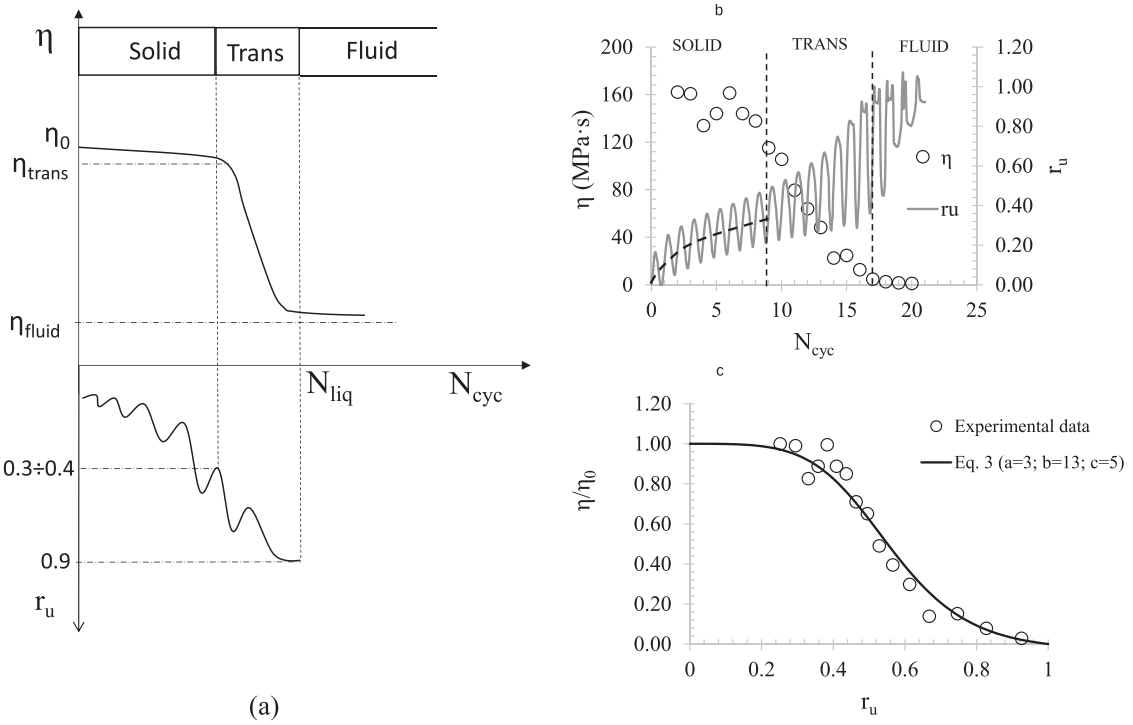

Fig. 3. Link between the apparent viscosity decay law and the pore pressure ratio: conceptual scheme (a), experimental results on Ticino sand (Mele, 2022) (b-c).

has been scheduled in order to analyse in detail the role of effective vertical stresses, loading paths (frequency, shape of loading, pre-existing shear stress), soil's fabric (moist tamped, air pluviated and undisturbed specimens) on the viscous behaviour of liquefiable sandy soils. The attention will be focused on the apparent viscosity decay law (Fig. 3a), viscosity-based excess pore water pressure generation model (Eq. (3)) and pseudo-plastic behaviour of liquefiable soils (Eq. (1)). Finally, the viscosity based excess pore water pressure model (Eq. (3)) and the proposed correlations to estimate the *fluid consistency coefficient* k and the *liquidity index* n have been validated at full scale by using the results of 1D non-linear site response analysis of the case study of Scortichino (Italy), affected by extensive liquefaction phenomena during the 2012 earthquake.

2. Material and dataset

All cyclic simple shear tests (Table 2) have been performed on Pieve di Cento sand, whose grain size distribution curve and physical properties have been reported in Fig. 4 and Table 1, respectively. Pieve di Cento (PdC) sand was retrieved from the field trial (Flora et al., 2021) of the European project LIQUEFACT. It is located in Emilia Romagna Region (Italy). All cyclic tests have been carried out using a sophisticated simple shear apparatus, where specimens are enclosed by flexible boundaries (Mele, 2023) and confined by pressurized water (cell pressure). Cylindrical specimens (d = 70 mm and h = 26 mm) have been prepared by moist tamping (MT) and air pluviation (AP) techniques. In the first case, dry sand is initially mixed with water that represents 5 % water content of the specimen. Then, the moist sand is compacted into two layers

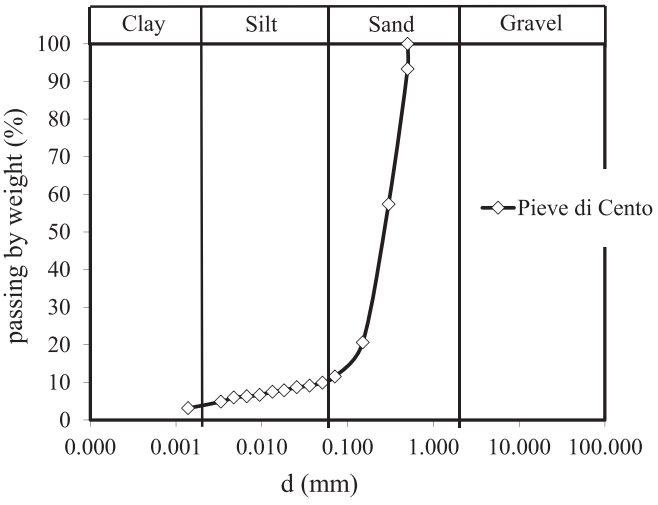

Fig. 4. Grain size distribution curve of Pieve di Cento sand.

Table 1
Physical properties of Pieve di Cento sand.

G_s	2.655
$e_{max} - e_{min}$	0.884 – 0.442
D_{50} (mm)	0.30
U_c	5.0
FC (%)	11

inside a split mould. Each layer is compacted into a designated portion of the required dry unit weight of the specimen. As known (Kwan, & El Mohtar, 2018), this technique has the advantage of reconstituting the specimens with a wide range of D_r ($7 \leq D_r$ (%) ≤ 75). Regarding the air pluviation, the dry sand is discharged vertically in air from a nozzle of a funnel. As well-known, the obtained relative density of the reconstituted specimens depends both on the height of fall during the preparation and on the nozzle's dimensions. Mele (2020) showed that the nozzle's dimension, at least in the tested range ($4 \leq d$ (mm) ≤ 15), does not seem to influence D_r of the specimens, on the contrary, when the height of fall increases, D_r increases as well. The AP specimens have been prepared with a height of fall of 40 cm, to reach D_r of about 40 % (Mele, 2020). In both cases (MT or AP methods), the specimens have been saturated increasing the back-pressure until having a B-value higher than 0.95. After that, they have been consolidated in K_0-conditions at different effective vertical stresses ($40.5 \leq \sigma'_v$ (kPa) ≤ 205.8). The K_0-condition is simulated through a sophisticated control system: the horizontal stress (cell pressure) is imposed by operator through a linear-time function and the vertical piston moves in order to regulate axial strain (ε_a) in accordance with the volumetric strain (ε_v) evolution to maintain the condition $d\varepsilon_V/d\varepsilon_a = 1.0$ (i.e. $\varepsilon_r = 0$) and, therefore, the diameter constant. As a consequence, vertical stress changes in response to soil behaviour.

Although unavoidable oscillations of the radial strain around zero occur, Mele (2023) showed that they are low enough to assume the deformations belong to the elastic region. After consolidation, a cyclic load has been applied choosing different shear stress loading paths (sinusoidal, triangular, rectangular and sawthrooth waveforms) and load frequencies ($0.05 \leq f \leq 5$ Hz). Through an active height-control (ASTM D6528–17 (2017) and ASTM D8296-19 (2019)) the height of the specimen is kept constant. Since the height and volume are both constant (undrained tests), the cross-sectional area does not change, as well.

Some tests have been performed applying a pre-existing (drained) shear stress ($5 < \tau_s < 6$ kPa) on the horizontal plane of the specimen before the cyclic (undrained) phase. The amount of static shear stress has been quantified via the parameter α:

$$\alpha = \frac{\tau_s}{\sigma'_{v0}} \tag{5}$$

where σ'_{v0} is the vertical effective consolidation stress.

Three different values of α have been considered (0.10; 0.12; 0.13) in order to have three different conditions: $\tau_{cyc} > \tau_s$ (stress reversal; MT25_sin0.05 test); $\tau_{cyc} = \tau_s$ (MT26_sin0.05 test); $\tau_{cyc} < \tau_s$ (without stress reversal; MT27_sin0.05 test).

The experimental program has been summarized in Table 2: the tests have been named with the kind of specimen's preparation technique (MT, AP or Und for undisturbed specimens), adopted waveform (sin, tri, rect and sawt) and load frequency (f = 0.05, 0.5, 5 Hz).

3. Apparent viscosity decay law

In this section the role of several parameters affecting the soil apparent viscosity η (Table 2) has been investigated: effective vertical stress, relative density, CSR, soil's fabric, cyclic loading frequency, loading waveforms, and pre-existing static shear stress (α, Eq. (5).

3.1. Effect of effective vertical stress, relative density and CSR

The decay laws of η with the number of cycles N_{cyc} pertaining to cyclic simple shear tests carried out on some reconstituted specimens (moist tamping; MT) (Table 2) have been plotted in Fig. 5a, b: the specimens have been tested adopting the same loading path (frequency, shape and values of α) and different relative densities (D_r) and confining stresses (σ'_{v0}). Experimental results confirm the trend already shown in Fig. 2a, with the apparent viscosity that decreases as the number of cycles (N_{cyc}) increases. The apparent viscosity decay law η-N_{cyc} is mainly affected by the applied CSR: when CSR increases the slope of the curve increases as well, reaching liquefaction after a lower number of cycles. The results agree with those reported by Qin et al. (2023).

Regarding to the link between the viscosity and the excess pore water pressure build up, Fig. 6a clearly shows that the transition phase starts in correspondence of $r_u \approx 0.40$ (inflection point): it means that when the excess pore pressure is about 40 % of the initial effective vertical stress the soil starts to change its state, moving away from the solid condition. The experimental data overlap each other in $r_u - \eta/\eta_0$ plane (Fig. 6), highlighted that σ'_{v0}, D_r and CSR have a negligible influence on the viscosity-based excess pore water pressure generation model (Eq. (3)). The parameters *a*, *b* and *c* of Eq. (3) have been therefore calibrated to have the best fitting with the experimental CSS test results (a = 2.31; b = 2.76; c = 5.34, Fig. 6).

3.2. Effect of frequency

Being the earthquakes characterized by frequencies (f = 1 ÷ 10 Hz) higher than those generally applied at the laboratory scale, three tests (MT3_sin0.05, MT16_sin0.5 and MT17_sin5, Table 2) have been carried out to investigate the effect of frequency on the apparent viscosity. All of them have been performed on moist tamped specimens consolidated at low effective vertical stresses ($56 \leq \sigma'_{v0} \leq 60$ kPa) and loaded by a (sinusoidal) cyclic load (CSR ≈ 0.10–0.115, Table 2) applied with frequency ranges from 0.05 to 5 Hz. Being the apparent viscosity decay laws linked to the strain rate (Eq. (2)), the adopted frequency has a relevant effect and lower values of η have

Table 2
Dataset of examined tests.

Test	Preparation technique	e_0	D_r (%)	σ'_{h0} (kPa)	σ'_{v0} (kPa)	α	Waveform	f (Hz)	CSR	Ref.
MT1_sin0.05	MT	0.683	45	27.2	58.6	0	Sinusoid	0.05	0.130	Mele, 2020
MT2_sin0.05	MT	0.670	48	18.7	53.4	0	Sinusoid	0.05	0.120	
MT3_sin0.05	MT	0.657	51	30.4	59.7	0	Sinusoid	0.05	0.115	
MT4_sin0.05	MT	0.574	70	25.2	49.7	0	Sinusoid	0.05	0.130	
MT5_sin0.05	MT	0.587	67	23.8	51.5	0	Sinusoid	0.05	0.140	
MT6_sin0.05	MT	0.854	7	24.3	52.0	0	Sinusoid	0.05	0.110	Mele et al., 2023b
MT7_sin0.05	MT	0.827	13	33.4	57.1	0	Sinusoid	0.05	0.110	
MT8_sin0.05	MT	0.583	68	21.2	59.9	0	Sinusoid	0.05	0.130	
MT9_sin0.05	MT	0.561	73	40.2	98.4	0	Sinusoid	0.05	0.140	
MT10_sin0.05	MT	0.691	43	52.1	106.5	0	Sinusoid	0.05	0.120	
MT11_sin0.05	MT	0.686	45	96.6	205.8	0	Sinusoid	0.05	0.130	
MT12_sin0.05	MT	0.553	75	85.0	198.0	0	Sinusoid	0.05	0.140	
Und13_sin0.05	Und_GP (*)	0.655	–	23.2	60.4	0	Sinusoid	0.05	0.12	Flora et al., 2021
Und14_sin0.05	Und_GP (*)	0.692	–	13.3	40.5	0	Sinusoid	0.05	0.110	
Und15_sin0.05	Und_O (*)	0.613	–	19.6	51.3	0	Sinusoid	0.05	0.130	
MT16_sin0.5	MT	0.673	48	29.1	55.7	0	Sinusoid	0.5	0.110	This study
MT17_sin5	MT	0.678	46	29.0	57.2	0	Sinusoid	5	0.100	
MT18_tri0.05	MT	0.693	43	28.3	44.6	0	Triang	0.05	0.120	
MT19_rec0.05	MT	0.701	41	40.0	54.6	0	Rectang	0.05	0.125	
MT20_swt0.05	MT	0.693	43	28.9	49.1	0	Sawtooth	0.05	0.120	
AP21_sin0.05	AP	0.673	48	35.7	66.2	0	Sinusoid	0.05	0.080	
AP22_sin0.05	AP	0.654	52	19.7	69.9	0	Sinusoid	0.05	0.085	
AP23_sin0.05	AP	0.675	47	34.1	68.9	0	Sinusoid	0.05	0.100	
AP24_sin0.05	AP	0.643	54	26.4	61.3	0	Sinusoid	0.05	0.105	
MT25_sin0.05	MT	0.700	42	24.1	53.0	0.10	Sinusoid	0.05	0.120	
MT26_sin0.05	MT	0.700	42	30.6	53.9	0.12	Sinusoid	0.05	0.125	
MT27_sin0.05	MT	0.708	40	32.7	49.8	0.13	Sinusoid	0.05	0.120	

(*) GP = Gel-Pusher; O = Osterberg. Not having enough quantities of soils, it was not possible to evaluate e_{max} and e_{min} (ASTM D4253–06 (2006); ASTM D4254–06 (2006)).

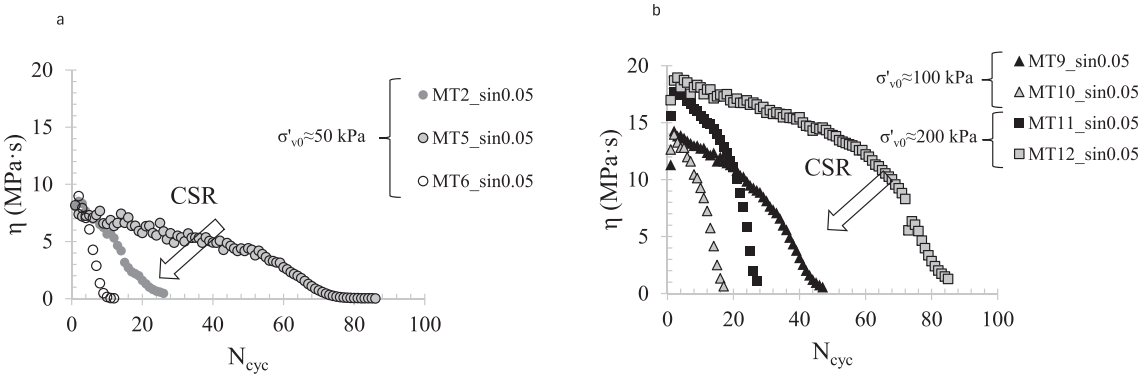

Fig. 5. Apparent viscosity decay curves for reconstituted specimens (MT) consolidated at lower (σ'_{v0}≈50 kPa) (a) and higher (σ'_{v0}≈100 and 200 kPa) (b) effective vertical stresses.

been obtained for higher frequencies (Fig. 7a). Indeed, for higher frequencies the apparent viscosity exhibits lower values, since the shear strain rate ($\dot{\gamma}$) is higher (see, Eq. (2). The effect of frequency disappears in the normalized $r_u - \eta/\eta_0$ plane (Fig. 7b): the theoretical curve previously shown in Fig. 6a (obtained via Eq. (3), with a = 2.31; b = 2.76; c = 5.34) fits well the experimental data of tests performed at different frequencies, suggesting that a unique curve can predict the behaviour of the tested soil.

3.3. Effect of loading waveform

In order to investigate the effect of the shape of loading on the apparent viscosity η, three additional cyclic simple shear tests have been carried out (MT18_tri0.05, MT19_rec0.05 and MT20_swt0.05, Table 2), applying a triangular (tri), rectangular (rec) and sawtooth (swt) waveform, respectively (Fig. 8). All of them have been carried out with the same value of CSR adopted in the test

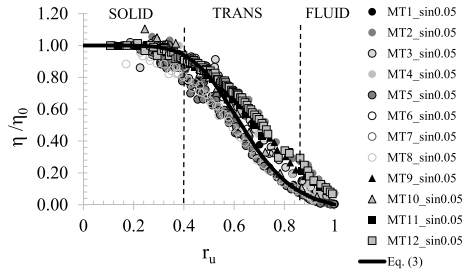

Fig. 6. Relationship between r_u and η/η_0 for some CSS tests on Pieve di Cento sand.

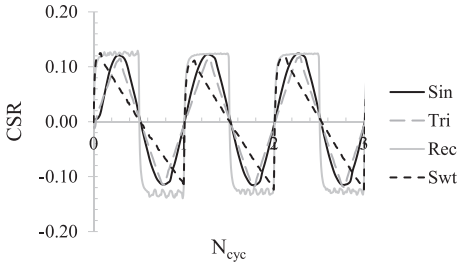

Fig. 8. Loading waveforms for cyclic tests: sinusoidal; triangular; rectangular and sawtooth (CSR = 0.12).

MT2_sin0.05 test (CSR = 0.12), performed by applying a sinusoidal waveform (Table 2).

The apparent viscosity decay curves have been plotted in Fig. 9a: it is worth noting that the values of η are affected by the shape of loading due to different strain rates. To better understand the waveform effect, in Fig. 9b the maximum and minimum shear strain rate per cycle has been plotted with r_u for the four tests. It can be noted that the difference between $\dot{\gamma}_{max}$ and $\dot{\gamma}_{min}$ is higher for MT19_rec0.05 test, performed with a rectangular waveform, where a sudden increase (or decrease) of loading is imposed. As a consequence, in this test η is lower than that pertained to the other ones (Fig. 9a). Moreover, due to the fact that $\dot{\gamma}$ is roughly constant with r_u (Fig. 9b), the decay curve is flatter compared to those of other tests (Fig. 9a). Therefore, a different response of MT19_rec0.05 test can be also observed in Fig. 9c, where the viscosity-based excess pore pressure generation model (Eq. (3)) calibrated on experimental data obtained by cyclic tests carried out with sinusoidal waveforms has been reported.

Lower values of shear strain rate in MT18_tri0.05 test are responsible of higher η compared to other tests (Fig. 9a). Asymmetrical values of $\dot{\gamma}$ are recorded in sawtooth waveform ($\dot{\gamma}_{max} > |\dot{\gamma}_{min}|$; Fig. 9b). The difference between $\dot{\gamma}_{max}$ and $\dot{\gamma}_{min}$ is higher than that computed in sinusoidal and triangular waveforms, therefore lower η values are exhibited in MT20_swt0.05 test (Fig. 9a).

The experimental results plotted in Fig. 9c show that the traditional S-shape of the relationship $r_u - \eta/\eta_0$ is not completely explicated (the fluid phase is not evident) for the other tested waveforms and a simpler power function (b = 0) could be suitable to fit these results (Fig. 9d). This experimental evidence implies that in a real case, where the seismic irregular input motion is expected, Eq. (3) could be simplified as follows:

$$\frac{\eta}{\eta_0} = 1 - r_u^a \tag{6}$$

In this way, only one parameter (*a*, Eq. (6)), should be calibrated (Fig. 9d). It is worth specifying that the parameter *a*, reported in Eq. (6), can be easily calibrated from simpler cyclic tests performed with sinusoidal waveforms. No need to perform tests with different waveforms. It makes easier the calibration of Eq. (6) from laboratory tests.

3.4. Effect of soil fabric

It is well known that the technique used to prepare the specimens can affect liquefaction behaviour of sandy soils (Mulilis et al., 1977). The effect is due to a different distribution of grain contacts (soil fabric) that develops during the preparation: generally, air pluviated specimens (AP) exhibit liquefaction resistance lower than that pertaining

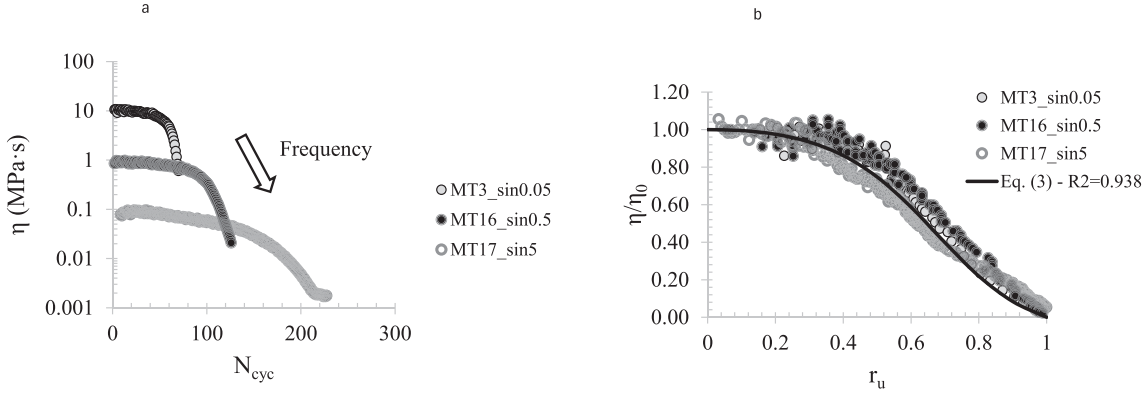

Fig. 7. Effect of frequency on the apparent viscosity decay curves (a) and on the relationship between r_u and η/η_0 (b).

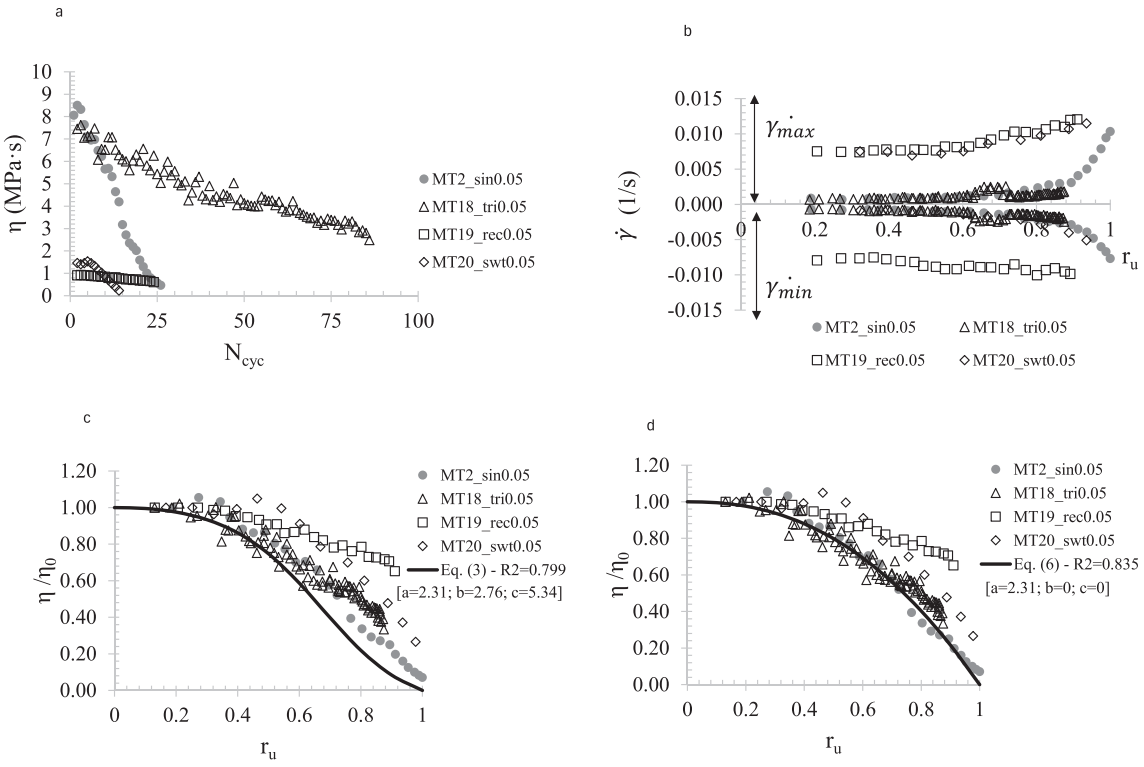

Fig. 9. Effect of waveform on the apparent viscosity decay curve (a) on the shear strain rate (b) on the relationship between r_u and η/η_0 compared with the theoretical Eq. (3) (c) and Eq. (6) (d) for Pieve di Cento sand.

to moist tamping ones (MT). In this section the results of four additional tests (AP21, AP22, AP23 and AP24, Table 2) carried out on specimens reconstituted with air pluviation method and three tests on undisturbed specimens (Und13_sin0.05, Und14_sin0.05, Und 15_sin0.05), have been compared to better understand the effect of soil fabric. For all of them, the apparent viscosity decay curves resemble the theoretical trend reported in Fig. 3a. Plotting the data in $r_u - \eta/\eta_0$ plane, it can be noted that the decay law is not affected by soil fabric: the theoretical curve (Eq. (3)); a = 2.31; b = 2.76; c = 5.34, Fig. 10b) obtained for MT specimens well fits the experimental data of AP and undisturbed specimens ($R^2 = 0.957$).

3.5. Effect of static shear stress

The existence of an initial static shear stress can have a significant effect on the cyclic strength or liquefaction potential of sandy soils. This aspect is relevant in many practical applications involving earth dams and slopes (i.e. Harder & Boulanger, 1997; Yang & Sze, 2011a-b; Pan & Yang, 2018; Sivathayalan & Ha, 2011; Tomasello & Porcino, 2022), or built environment (i.e. Dashti et al., 2010; Bertalot & Brennan, 2015; Adamidis & Madabhushi, 2018).

In order to verify the effect of the static shear stress on the apparent viscosity, three additional simple shear tests

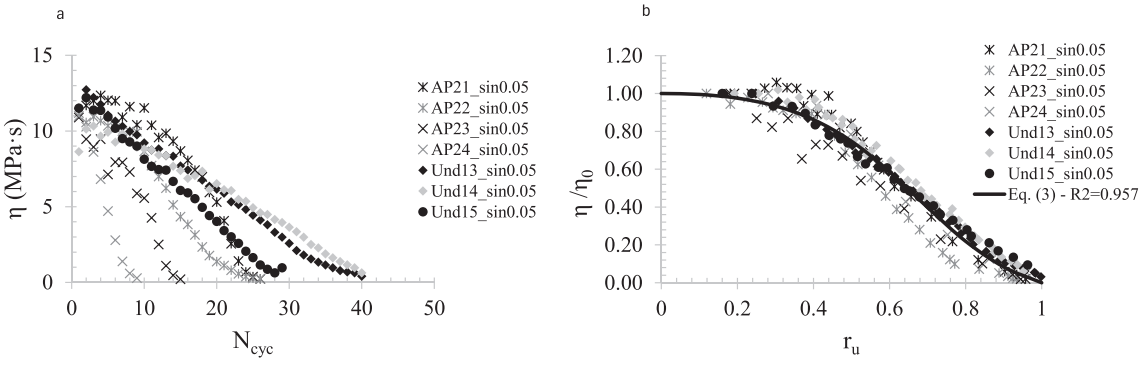

Fig. 10. Effect of soil fabric on the apparent viscosity decay curve (a) on the relationship between r_u and η/η_0 (b) for Pieve di Cento sand.

have been performed by imposing the same value of CSR (Table 2) and different values of α (eq.5). The results are shown in the planes $\sigma'_v - \tau$ (Fig. 11a, c, e) and $N_{cyc} - r_u - \gamma$ (Fig. 11b, d, f). It can be noted that the stress-paths of all tests move towards the failure line of Pieve di Cento sand ($\tau/\sigma' = 0.60$, Mele, 2023) inducing plastic shear strain accumulation (Yang & Sze, 2011a) toward the positive side (Fig. 11b, d, f).

The apparent viscosity decay curves are reported in Fig. 12: it is worth noting that the final value of η is affected by the adopted value of α. It is due to the fact that when the value of α increases the shear strain rate decreases, and then η exhibits higher values (Eq. (2)). Moreover, when *non-stress reversal condition* occurs (Fig. 11e), the fluid phase could be not fully-explicated (Fig. 11f, where the $r_u < 0.9$). This is evident plotting the results in the $\eta/\eta_0 - r_u$ plane: the theoretical curve (Eq. (3), Fig. 12b) well fits the experimental data up to $r_u = 0.60$, while for higher values of r_u the approximate curve is below the experimental results pertaining to cyclic tests with higher value of α (MT27_sin0.05).

4. Pseudo-plastic behaviour

As previously mentioned, when liquefaction phenomenon is triggered, the sudden drop of the value of the apparent viscosity (Fig. 3a) reveals the change of state of the soil from solid to a pseudo-plastic liquid. When, it occurs, the rheological behaviour of liquefied soils can be simulated through Eq. (1). In Fig. 13 the results of cyclic tests carried out on reconstituted moist tamped specimens have been plotted in $\dot{\gamma}$-η plane, where $\dot{\gamma}$ has been computed as the average value between $\dot{\gamma}_{max}$ and $|\dot{\gamma}_{min}|$ for each cycle. As for cyclic triaxial tests, also for cyclic simple shear tests,

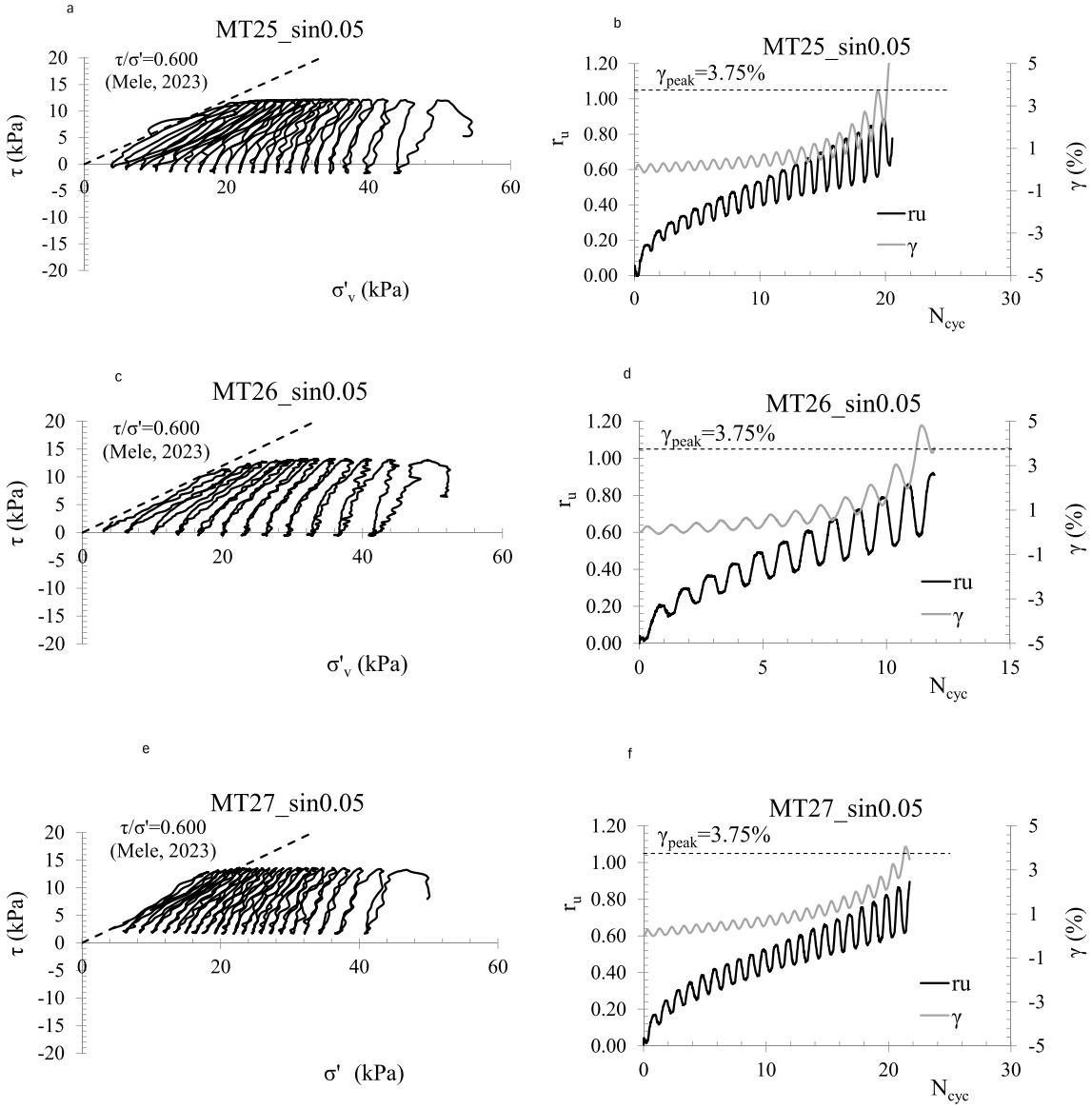

Fig. 11. Simple shear tests performed with a static shear stress in the planes $\sigma'_v - \tau$ (a, c, e) and N_{cyc} with r_u and γ (b, d, f).

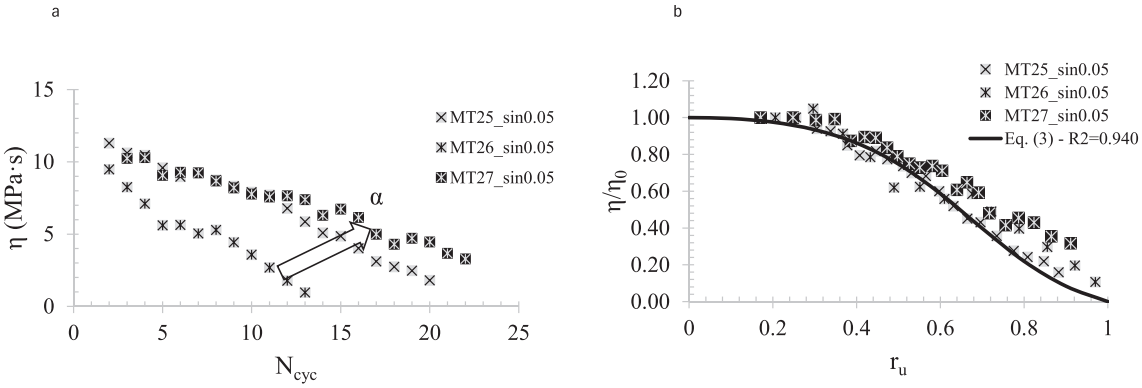

Fig. 12. Effect of pre-existing static shear stress on the apparent viscosity decay curve (a) and on the relationship between r_u and η/η_0 (b) for Pieve di Cento sand.

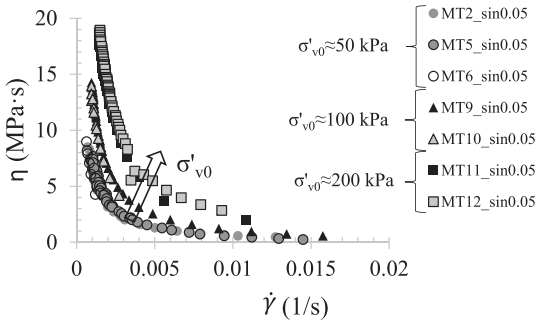

Fig. 13. Effect of σ'_{v0} on the relationship between $\dot{\gamma}$- η for Pieve di Cento sand.

the power law between the apparent viscosity (η) and the shear strain rate ($\dot{\gamma}$) (Eq. (1)) correctly simulates the behaviour of sand. It can be noted that the effect of the confining stress σ'_{v0} is relevant: specimens consolidated with higher σ'_{v0} (Table 2) exhibit higher curves compared to those carried out with lower values of effective vertical stress ($\sigma'_{v0} \approx 50$ kPa, Table 2).

The parameters *k* and *n* of Eq. (1) (*fluid consistency coefficient* and *liquidity index*, respectively) have been calibrated for each test (Table 2) to have the best fitting with the experimental data. In Fig. 14a and Fig. 14c, k and n values have been plotted for each test together with the upper and lower bounds proposed by Mele (2022): it can be observed that the experimental results of the tests performed at higher confining stresses (MT11_sin0.05 and MT12_sin0.05 tests) are outside the theoretical bounds reported in Fig. 2b and Fig. 2c. More relevant differences between experimental results reported in this paper and the approximate relationship proposed in Fig. 2c, can be noted in Fig. 14c. To stress out the effect of σ'_{v0}, the experimental data have been plotted in the plane CSR – k/σ'_{v0} in Fig. 14b and k/σ'_{v0} – n plane in Fig. 14d, together with the experimental data of cyclic triaxial tests reported by Mele (2022). New regression functions have been identified for the fluid consistency coefficient (*k*) and liquidity index (*n*), that well fit data of triaxial tests of Mele (2022), as well. This result seems to suggest that the calibration of *k* and *n* is independent on the kind of performed tests. It is probably due to the fact that when the transition phase starts (Fig. 3a) the soil loses memory of its original state and as a consequence, the behaviour is not yet affected by the applied loading paths.

This aspect is even clearer in Fig. 15, in which the effect of stress path history (load frequency, waveforms and pre-existing static shear stress) or the fabric effect (MT, AP or undisturbed specimens) on the pseudo-plastic behaviour of soils (Eq. (1)) has been investigated. Once again, the reliability of the Eq. (1) is confirmed and the proposed correlations to estimate k and n (Fig. 14b-d) allow to well predict the pseudo-plastic behaviour of sandy soils ($R^2 > 0.883$). It should be specified that the predicted curves have been obtained assuming average values of σ'_{v0} and CSR for the examined group of tests.

5. The case study of Scortichino (Italy)

The outcomes of the experimental study shown in §3 and §4 highlight the effectiveness of the apparent viscosity in representing the change in soil state during the liquefaction phenomenon. The processing of the laboratory data with a viscous perspective has allowed to derive analytical relationships able to predict the earthquake induced excess pore water pressure build up and also the behaviour of liquefied soils as pseudo-plastic fluids. The findings have been extended to a large scale, analysing the site of Scortichino located in the large area of the river Po valley (Emilia Romagna region, Northern Italy) hit by the seismic sequence of May 2012. The damage survey carried out after the seismic event revealed liquefaction evidence (Tonni et al., 2015; Chiaradonna et al., 2019), such as sand boils and lateral spreading mechanisms. The site of Scortichino was studied in depth performing an extensive experimental program, composed by laboratory and in-situ tests, in order to define accurately the geotechnical model (Tonni et al., 2015). The stratigraphic model of the most damaged section (named c-c') is composed mainly by four deposits: dyke, composed by subsequent layers of sand, sandy silt

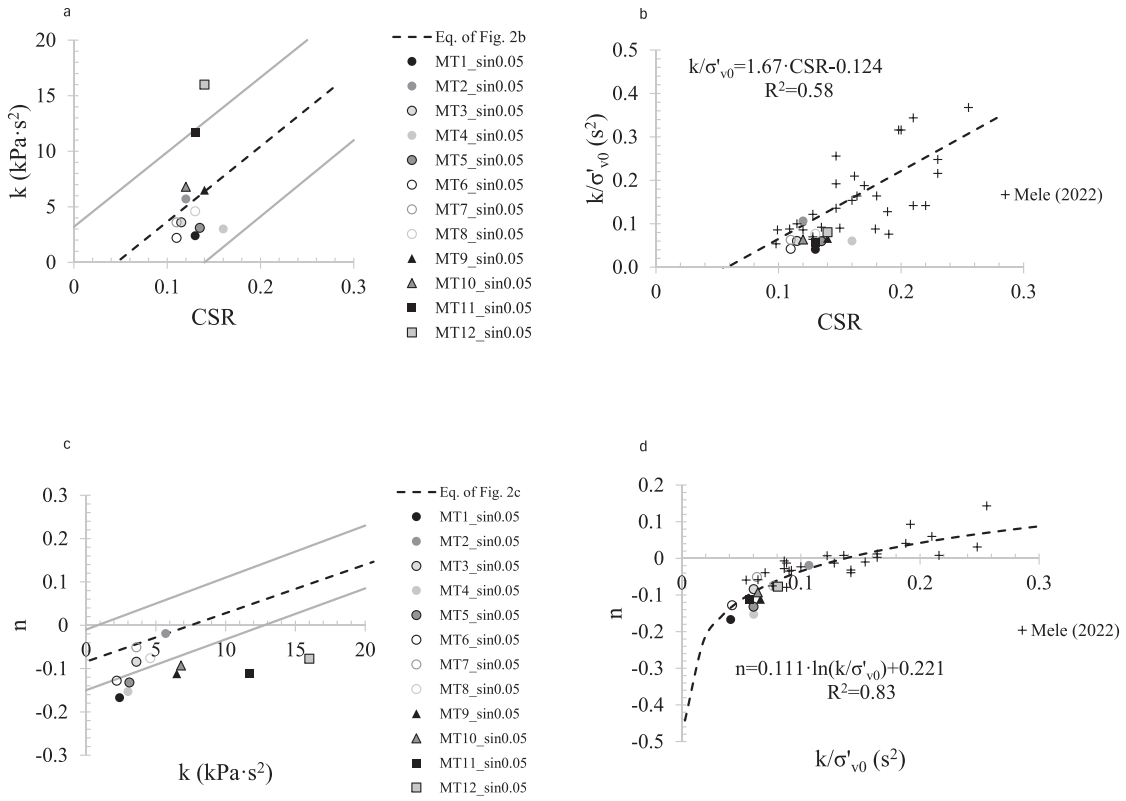

Fig. 14. Relationships CSR – k (a) and k – n (c) and their modification to consider the effect of σ'_{v0} in the plane CSR – k/σ'_{v0} (b) and k/σ'_{v0} – n (d).

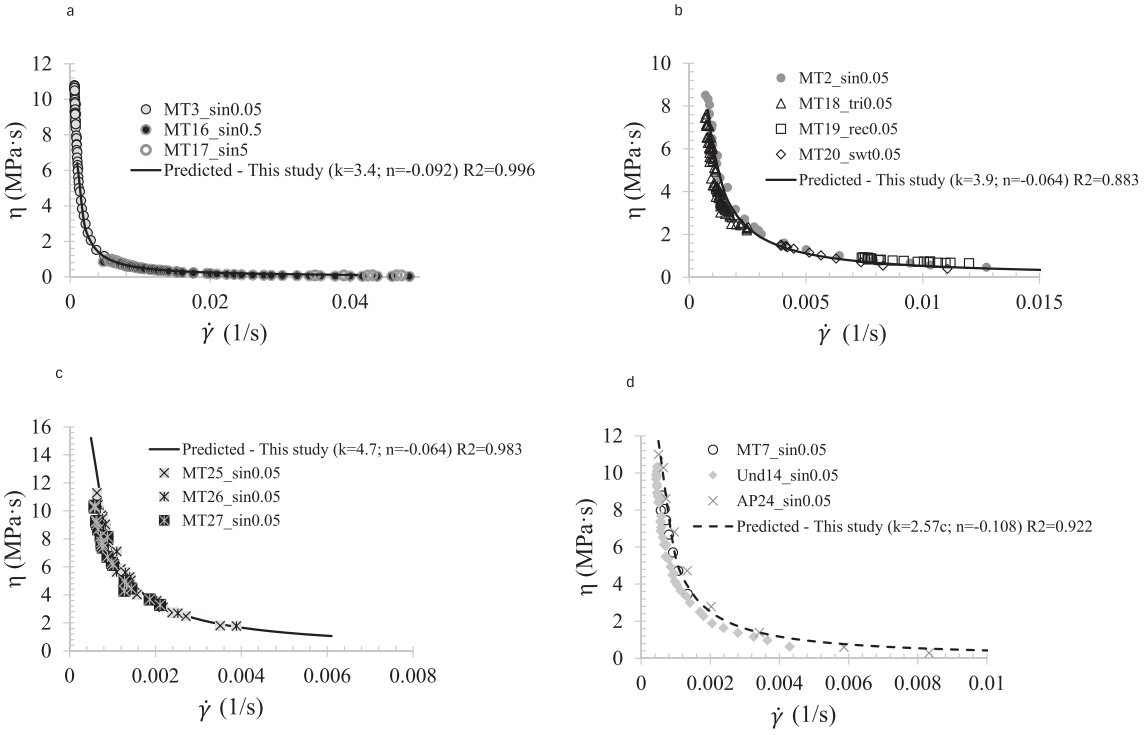

Fig. 15. Effect of frequency (a), waveform (b), pre-existing shear stress (c) and fabric effect (d) on the pseudo-plastic behaviour of Pieve di Cento sand and comparisons with predicted behaviour.

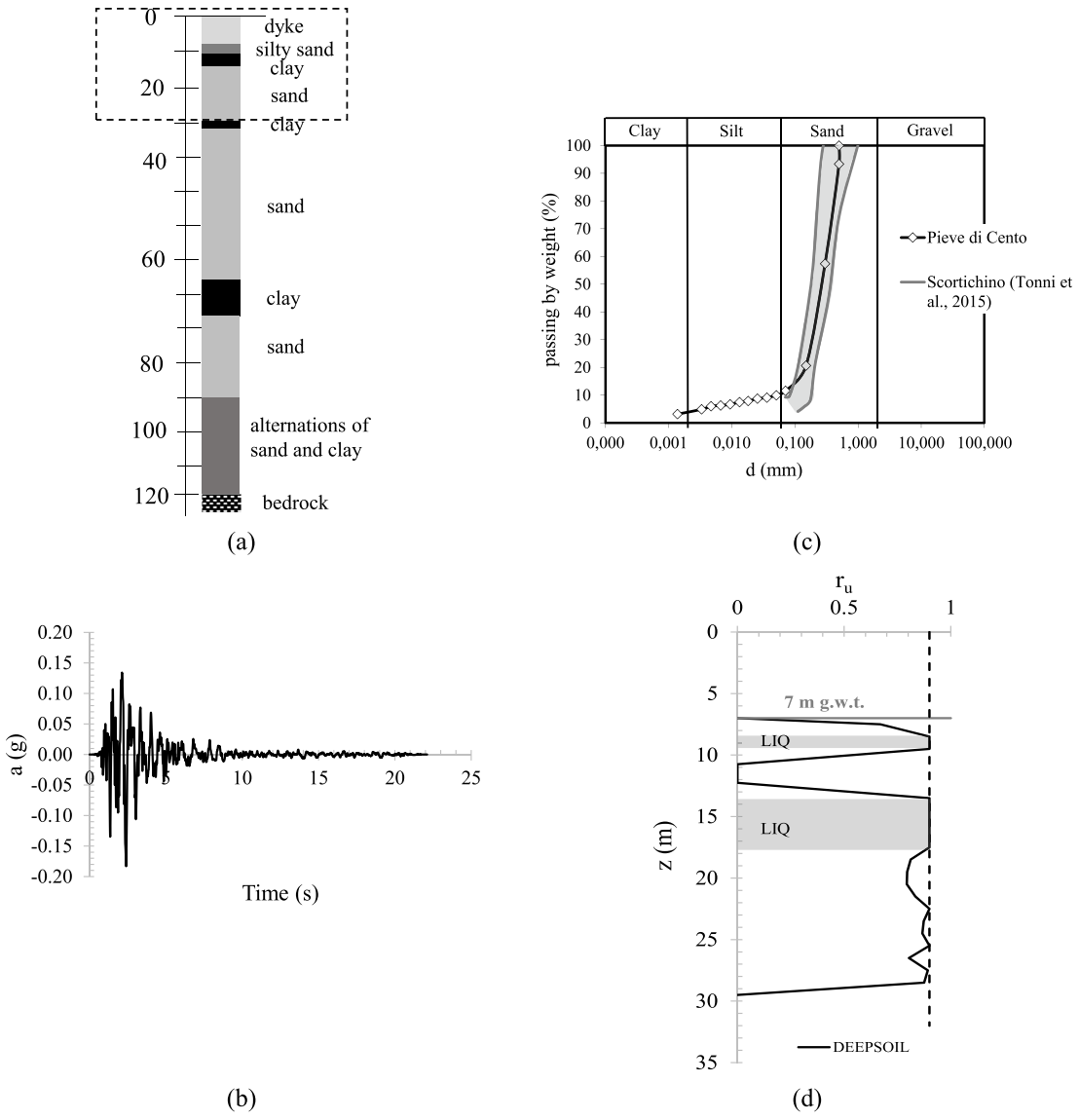

Fig. 16. Subsoil profile of Scortichino (a), input motion (b), comparison between Pieve di Cento and Scortichino sands (c) and r_u profile (d).

and silty sand; silty sand; sand and clay (Fig. 16a; Tonni et al., 2015).

A 1D non-linear site response analysis has been performed by means of DEEPSOIL (Hashash et al., 2020) with an input motion applied at bedrock, modelled as an elastic half-space. Since no acceleration records were available at the site of Scortichino, a selection of recorded accelerograms was adopted in order to simulate the 20th May event. As reported by Chiaradonna (2016), the input motion was defined through a selection of records within the Italian database ITACA, based on the magnitude (5.5–6.5) and distance (5 – 10 km) bins approach. The NS component of the main shock of Irpinia earthquake (11/23/1980), recorded at the Lauria station was finally selected and adopted as input motion in the analyses. The selected time history was then scaled to the PGA estimated at the site through the hazard map (PGA = 0.192 g; Fig. 16b).

The pore pressure energy-model of Berrill & Davis (1985), already implemented in DEEPSOIL, has been used to predict the r_u profile (Fig. 16d). This model does not need the complex conversion in an equivalent number of cycles but requires the calibration of two parameters. They have been calibrated on the results of in situ tests according to the simple procedure suggested by Mele et al. (2023a). It should be mentioned that the analysis has been performed in terms of effective stresses with a loosely coupled approach.

Four depths have been analysed in detail: z = 7.5, 9.5, 15.5 and 17.5 m from ground surface. In the shallowest one, no liquefaction occurs as shown by the value of r_u lower than 0.90 (r_u = 0.67, Fig. 16d). On the contrary, in the layers located at 9.5, 15.5 and 17.5 the liquefaction occurs, as demonstrated by the attained values of pore pressure ratio r_u (r_u = 0.90, Fig. 17c).

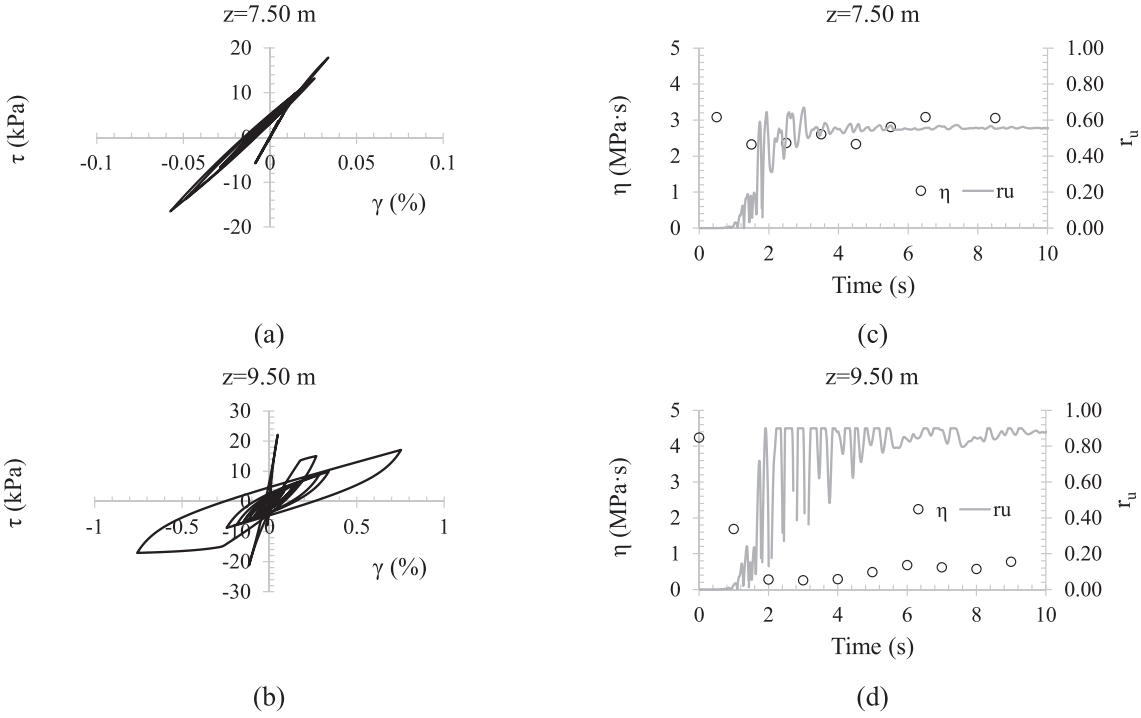

Fig. 17. Results of DEEPSOIL: stress–strain cycles (a, b), pore pressure ratio and apparent viscosity with time (c, d) of two layers.

As an example in Fig. 17, the stress–strain cycles (Fig. 17a-b) and the pore pressure ratio with time (Fig. 17-c-d) returned by DEEPSOIL have been plotted for layers at 7.5 and 9.5 m.

The results returned by DEEPSOIL, in the first 10 s and at the four selected depths have been interpreted from a viscous point of view. Firstly, the apparent viscosity has been calculated via Eq. (2) with the following steps:

1) from the time history of shear stress, τ_{max} and τ_{min} in each second have been considered;
2) from the time history of shear strain, shear strain rate has been computed as $\Delta\gamma/\Delta t$. As for τ, $\dot{\gamma}_{max}$ and $\dot{\gamma}_{min}$ have been selected in each second;
3) known τ_{max}, τ_{min}, $\dot{\gamma}_{max}$ and $\dot{\gamma}_{min}$ η can be calculated for each second (Fig. 17c-d).

Comparing the time history of η at 7.50 and 9.50 m (Fig. 17c-d), it can be observed that η is roughly constant in the shallowest layer (Fig. 17c), since no liquefaction is attained. On the contrary, a sudden drop of η occurs at 9.50 m when r_u approaches to 0.90 (attainment of liquefaction).

In Fig. 18, η/η_0 has been plotted with the maximum value of r_u in each second for each examined depth. Data have been compared with the theoretical curves obtained for sinusoidal (Eq. (3)) and non-sinusoidal waveforms (Eq. (6)), where the parameters *a*, *b* and *c* have been calibrated on the results of laboratory tests on Pieve di Cento sand (being the two sands very similar, Fig. 16c).

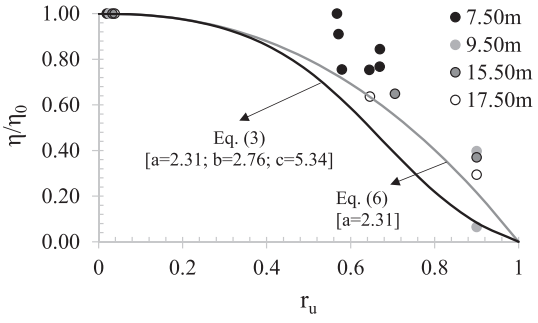

Fig. 18. Data of 1D non-linear analysis of Scortichino processed with a viscous approach in r_u-η/η_0 plane, compared with the proposed Eqs. (3) and (6) to predict pore pressures.

Although a data dispersion can be noted for z = 7.50 m, due to some fluctuation of η (Fig. 17c), Fig. 18 confirms that for irregular loads (real cases) Eq. (6) should be preferred to predict more accurately the earthquake induced excess pore water pressure. With this simple relationship, only one parameter (*a*) must be calibrated from laboratory tests (note that the parameter *a* has been calibrated from the sinusoidal waveform tests). The good agreement between the estimated pore pressure (Eq. (6)) and the results of 1D-non linear site response analysis seem to suggest that viscosity-based pore generation model could be used to predict the excess pore water pressure generated during seismic loading. The reliability of the model should be confirmed by more data, however the preliminary results seem to be very promising. Likewise energy-based

Table 3
Calibration of the pseudo-plastic parameters of Scortichino soils (eq.1).

Depth (m)	CSR(*)	k/σ'_{v0} (s^2)	k (kPa·s^2)	n
9.50	0.104	0.0503	6.92	−0.111
15.50	0.089	0.0250	4.81	−0.188
17.50	0.083	0.0236	5.02	−0.195

(*) $CSR = 0.65 \cdot \tau_{max}/\sigma'_{v0}$.

pore pressure generation models, the viscosity-based model does not require conversion in equivalent number of cycles of uniform shear stress. It is based on a more comprehensive consideration of the cyclic stress–strain behaviour of soils. Moreover, the implementation in numerical code could be easy.

5.1. Pseudo-plastic behaviour

The effectiveness of the correlations between $k/\sigma'_{v0} - CSR$ and $k/\sigma'_{v0} - n$ provided in section 4, has been tested for the case study of Scortichino. The cyclic stress ratio CSR at different depths has been quantified through the simple procedure proposed by Seed & Idriss (1970), while the *fluid consistency coefficient* (k) and *liquidity index* (n) have been estimated via the regressions reported in Fig. 14 b,d (Table 3). The knowledge of k and n allows the prediction of the pseudo-plastic behaviour of the liquefied soils through Eq. (1).

In Fig. 19 the results of the dynamic analysis in terms of η-$\dot{\gamma}$ have been plotted for the examined depths where liquefaction occurs (z = 9.50, 15.50 and 17.50 m) and compared with the prediction given by Eq. (1). The comparison highlights the effectiveness of the prediction in all the depths in which liquefaction is triggered. The proposed procedure to estimate k and n, seems to be consistent. It can be used as a powerful tool to model the behaviour of liquefied sands.

6. Concluding remarks

In this paper, the behaviour of liquefiable soils has been investigated through the *apparent viscosity*, that is a physically based parameter which well represents the temporary state change induced by liquefaction phenomenon. A large experimental program (Table 2) allowed to derive an innovative viscosity-based excess pore pressure generation model that has the advantage not to need the complex conversion of the seismic demand in an equivalent number of uniform cycles. The potential of the apparent viscosity as a parameter to model the pseudo-plastic behaviour of liquefied sandy soils has been analysed at small scale and after verified at large scale (§.5).

The main findings have been drawn out:

- The proposed *viscosity-based excess pore water pressure generation model* must be calibrated on experimental results carried out with cyclic tests on reconstituted or undisturbed soils. The experimental study revealed that the calibration is affected by the adopted waveform and the presence of a static shear stress. On the contrary, the

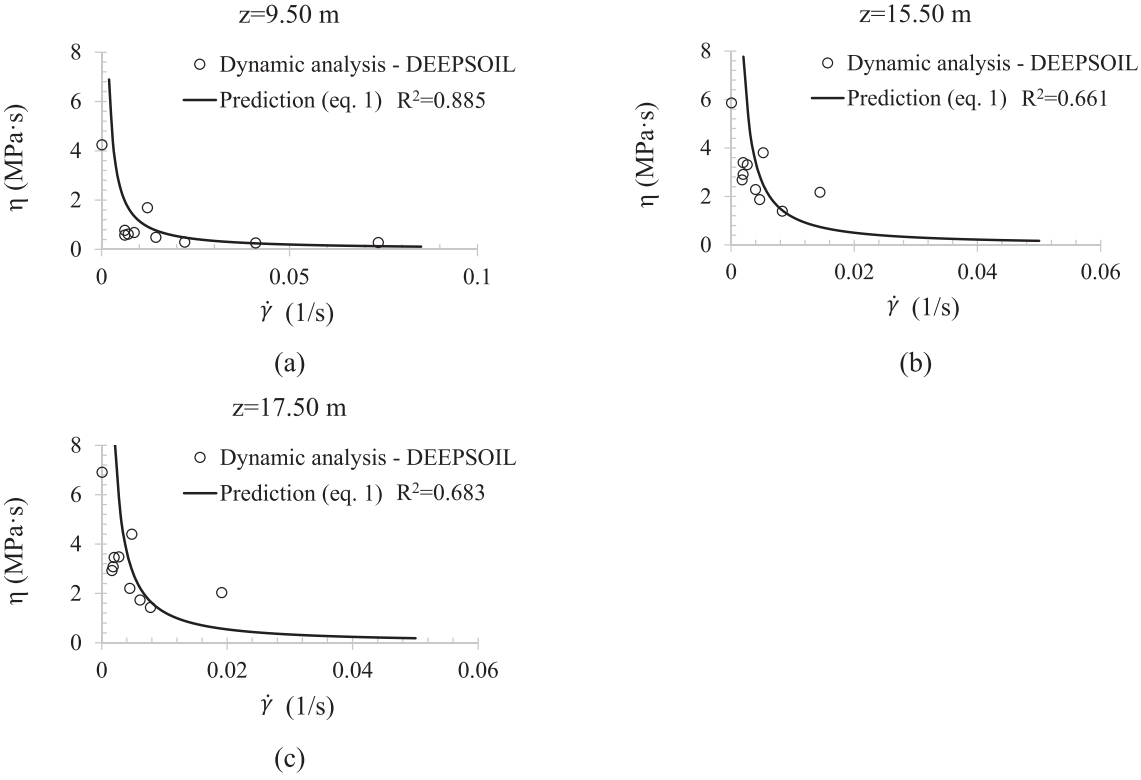

Fig. 19. Results of dynamic analysis in terms of η–$\dot{\gamma}$ compared with those predicted by the proposed method.

Table 4
Synthesis of parameters affecting the apparent viscosity.

Effect	Range/kind	Excess pore pressure generation model (Eq. (3))	Pseudo-plastic behaviour (Eq. (1))
Relative density (Dr)	$7 \leq D_r$ (%) ≤ 75	Negligible	Negligible
Cyclic Stress Ratio (CSR)	$0.08 \leq CSR \leq 0.16$	Negligible	Not – negligible
Effective vertical stress (σ'_{v0})	$40.5 \leq \sigma'_{v0}$ (kPa) ≤ 205.8	Negligible	Negligible
Fabric	Undisturbed; MT; AP	Negligible	Negligible
Frequency (f)	$0.05 \leq f$ (Hz) ≤ 5	Negligible	Negligible
Waveforms	Sinusoidal, triangular, rectangular and sawtooth	Not – negligible	Negligible
Static shear stress (τ_s)	$0.10 \leq \alpha \leq 0.13$	Not – negligible	Negligible

soil fabric, σ'_{v0}, D_r and CSR have a negligible influence on the calibration parameters (Table 4). The parameters of viscosity-based excess pore water pressure generation model can be calibrated to have the best fitting with the results of stress-controlled laboratory (cyclic triaxial or simple shear) tests with a sinusoidal waveform.

- The *pseudo-plastic behaviour of liquefied soils* is mainly affected by the effective vertical stress (Tab.4), while the other studied parameters (fabric, load path) have a negligible effect on the fluid consistency coefficient (k) and liquidity index (n). The proposed correlations shown in Fig. 14b-d allow to easily calibrate k and n starting from CSR at a generic depth. However, it is worth noting that the proposed relationships shown in Fig. 14b-d are valid for CSR higher than 0.06. Further tests should be performed with lower CSR to better investigate the trend of curves when lower cyclic stress amplitudes are applied.

Although, further tests should be performed, this paper can be considered as a preliminary work, which shows the potentiality of the apparent viscosity not only to model the behaviour of liquefied soils but also to predict the accumulation of the excess pore water pressure.

Data availability statement

Some or all data, models, or code that support the findings of this study are available from the corresponding author upon reasonable request.

CRediT authorship contribution statement

Lucia Mele: Conceptualization, Funding Acquisition, Data Curation, Writing - Original Draft, Investigation, Formal Analysis, Methodology. **Stefania Lirer:** Writing - Review & Editing, Supervision, Investigation. **Alessandro Flora:** Writing - Review & Editing, Supervision, Investigation.

Acknowledgement

The financial contribution of the of the following projects is gratefully acknowledged: DPC - RELUIS project (2022-2024), WP16: Contributi normativi – Geotecnica, Task 16.1 – Analisi della risposta sismica locale e liquefazione; Finanziamento Ricerca di Ateneo (FRA-2022) for the project "ASsessment of seismic Induced Settlements of Multi layered soils under shallow foundAtions and mItigation Risk actions" (SISMAIR).

References

Adamidis, O., Madabhushi, S.P., 2018. Deformation mechanisms under shallow foundations on liquefiable layers of varying thickness. Géotechnique 68 (7), 602–613.

ASTM D4253-06 2006. Standard test methods for maximum index density and unit weight of soils using a vibratory table", Annual Book of ASTM Standards, ASTM International, West Conshohocken, PA.

ASTM D4254-06 2006. Test methods for minimum index density and unit weight of soils and calculation of relative density, Annual Book of ASTM Standards, ASTM International, West Conshohocken, PA.

ASTM D6528-17 2017. Standard test method for consolidated undrained direct simple shear testing of fine grain soils. ASTM International: West Conshohocken.

ASTM D8296-19 2019. Standard test method for consolidated undrained cyclic direct simple shear test under constant volume with load control or displacement control.

Baris, A., Spacagna, R.L., Paolella, L., Koseki, J., Modoni, G., 2021. Liquefaction fragility of sewer pipes derived from the case study of Urayasu (Japan). Bulletin of Earthquake Engineering 19 (10), 3963–3986.

Berrill, J.B., Davis, R.O., 1985. Energy dissipation and seismic liquefaction of sands: revised model. Soils and Foundations 25 (2), 106–118.

Bertalot, D., Brennan, A.J., 2015. Influence of initial stress distribution on liquefaction-induced settlement of shallow foundations. Géotechnique 65 (5), 418–428.

Booker, J.R., Rahman, M.S., Seed, H.B. 1976. GADFLEA—a computer program for the analysis of pore pressure generation and dissipation during cyclic or earthquake loading. Earthquake Engineering Center, University of California, Berkeley.

Castiglia, M., de Magistris, F.S., Onori, F., Koseki, J., 2021. Response of buried pipelines to repeated shaking in liquefiable soils through model tests. Soil Dynamics and Earthquake Engineering 143 106629.

Chen, Y., Liu, H. 2011. Simplified method of flow deformation induced by liquefied sands. In Design, Construction, Rehabilitation, and Maintenance of Bridges (pp. 160-167).
Chen, Y.M., Liu, H.L., Zhou, Y.D., 2006. Analysis on flow characteristics of liquefied and post-liquefied sand. Chinese Journal of Geotechnical Engineering 28 (9), 1139–1143.
Chen, G., Zhou, E., Wang, Z., Wang, B., Li, X., 2016. Experimental study on fluid characteristics of medium dense saturated fine sand in pre- and post-liquefaction. Bulletin of Earthquake Engineering 14 (8), 2185–2212.
Chiaradonna, A., 2016. Development and assessment of a numerical model for non-linear coupled analysis on seismic response of liquefiable soils. University of Napoli Federico II, Naples.
Chiaradonna, A., Tropeano, G., d'Onofrio, A., Silvestri, F., 2019. Interpreting the deformation phenomena of a levee damaged during the 2012 Emilia earthquake. Soil Dynamics and Earthquake Engineering 124, 389–398.
Chiou, J.S., Ng, J.L., 2022. Investigation of Newtonian and non-Newtonian Bingham fluid models for lateral flow simulation of liquefied soil. Ocean Engineering 266 112990.
Committee on Soil Dynamics of the Geotechnical Engineering Division, 1978. Definition of terms related to liquefaction. Journal of Geotechnical Engineering 104 (GT9), 1197–11120.
Cubrinovski, M., Bray, J.D., Taylor, M., Giorgini, S., Bradley, B., Wotherspoon, L., Zupan, J., 2011. Soil liquefaction effects in the central business district during the February 2011 Christchurch earthquake. Seismological Research Letters 82 (6), 893–904.
Dashti, S., Bray, J.D., Pestana, J.M., Riemer, M., Wilson, D., 2010. Mechanisms of seismically induced settlement of buildings with shallow foundations on liquefiable soil. Journal of Geotechnical and Geoenvironmental Engineering 136 (1), 151–164.
Dobry, R., Pierce, W.G., Dyvik, R., Thomas, G.E., Ladd, R.S., 1985. Pore pressure model for cyclic straining of sand. Civil Engineering Department, Rensselaer Polytechnic Institute, Troy.
Flora, A., Bilotta, E., Chiaradonna, A., Lirer, S., Mele, L., Pingue, L., 2021. A field trial to test the efficiency of induced partial saturation and horizontal drains to mitigate the susceptibility of soils to liquefaction. Bulletin of Earthquake Engineering 19 (10), 3835–3864.
Green, R.A., Mitchell, J.K., Polito, C.P., 2000. An energy-based pore pressure generation model for cohesionless soils. In: John Booker Memorial Symposium Developments in Theoretical Geomechanics, pp. 383–390.
Hamada, M., Wakamatsu, K., 1998. A study on ground displacement caused by soil liquefaction. Proc. Jpnsoc Civil Eng 1998 (596), 189–208.
Harder, Jr. L.F., Boulanger, R.W. 1997. Application of Kσ and Kα correction factors. In: Youd TL, Idriss IM, editors. Proceedings of the NCEER workshop on evaluation of liquefaction resistance of soils. Buffalo, N.Y.: National Center for Earthquake Engineering Research, State University of New York at Buffalo. p. 167–90.
Hashash, Y.M.A., Musgrove, M.I., Harmon, J.A., Ilhan, O., Xing, G., Numanoglu, O., et al., 2020. DEEPSOIL 7.0, user manual. Board of Trustees of University of Illinois at Urbana-Champaign, Urbana, IL.
Ishihara, K., 1993. Liquefaction and flow failure during earthquakes. Geotechnique 43 (3), 351–451.
Kwan, W.S., El Mohtar, C., 2018. A review on sand sample reconstitution methods and procedures for undrained simple shear test. International Journal of Geotechnical Engineering.
Lirer, S., Mele, L., 2019. On the apparent viscosity of granular soils during liquefaction tests. Bulletin and Earthquake Engineering. https://doi.org/10.1007/s10518-019-00706-0.
Lu, C.W., Lin, Y.F., Lee, W.L., Huang, L.Y., 2023a. The Impact of apparent viscosity on estimating liquefaction-induced settlement. Proceeding of the 21st Southeast Asian Geotechnical Conference and 4th AGSSEA Conference (SEAGC-AGSSEA 2023).
Lu, C.W., Lin, Y.F., Lee, W.L., 2023b. Liquefaction-induced manhole uplifting prediction coupling with a thixotropic fluid model. 16Th Japan Earthquake Engineering Symposium.
Mele, L., 2022. An experimental study on the apparent viscosity of sandy soils: from liquefaction triggering to pseudo-plastic behaviour of liquefied sands. Acta Geotechnica 17 (2), 463–481.
Mele, L., 2023. Experimental study with complete stress state interpretation of undrained monotonic and cyclic simple shear tests with flexible boundaries. Acta Geotechnica. https://doi.org/10.1007/s11440-023-01907-3.
Mele, L., Lirer, S., Flora, A. 2023b. Experimental investigation on the post-liquefaction behaviour of sands in simple shear conditions. Special Issue on Experimental Investigations from Very Small Strains to Beyond Failure for Geotechnical Testing Journal. Geotechnical Testing Journal. https://doi.org/10.1520/GTJ20230306.
Mele, L. 2020. Experimental and theoretical investigation on cyclic liquefaction and on the effects of some mitigation techniques (Doctoral dissertation, PhD Thesis, Università degli Studi di Napoli Federico II, Napoli, Italy).
Mele, L., Lirer, S., Flora, A., 2023a. A simple procedure to calibrate a pore pressure energy-based model from in situ tests. Acta Geotechnica. https://doi.org/10.1007/s11440-022-01650-1.
Miyajima, M., Kitaura, M., Koike, T., Hasegawa, M., 1995. Experimental study on characteristics of liquefied ground flow. In Earthquake. Geotechnical Engineering, 969–974.
Mulilis, J.P., Seed, H.B., Chan, C.K., Mitchell, J.K., Arulanandan, K., 1977. Effects of sample preparation on sand liquefaction. Journal of the Geotechnical Engineering Division 103 (2), 91–108.
Pan, K., Yang, Z.X., 2018. Effect of initial static shear on cyclic resistance and pore pressure generation of saturated sand. Acta Geotechnica. 13, 473–487. https://doi.org/10.1007/s11440-017-0614-5.
Qin, Y., Du, X., Yang, Z., Ma, W., Wu, Q., Chen, G., 2023. Characteristics of solid–liquid phase transformation of saturated coral sand subjected to various patterns of cyclic loading. Canadian Geotechnical Journal, (ja).
Sasaki, Y., Towhata, I., Tokida, K., Yamada, K., Matsumoto, H., Tamari, Y., Saya, S., 1992. Mechanism of permanent displacement of ground caused by seismic liquefaction. Soils and Foundations 32 (3), 79–96.
Schenkengel, K.U., Vrettos, C., 2014. Simulation of liquefied sand by the Lattice Boltzmann method. Geotechnik 37 (2), 96–104.
Seed, H.B., Idriss, I.M. 1970. Soil moduli and damping factors for dynamic response analysis. Report No EERC 70–10, University of California, Berkeley, California.
Sivathayalan, S., Ha, D., 2011. Effect of static shear stress on the cyclic resistance of sands in simple shear loading. Canadian Geotechnical Journal 48, 1471–1484. https://doi.org/10.1139/t11-056.
Tokimatsu, K., Asaka, Y., 1998. Effects of liquefaction-induced ground displacements on pile performance in the 1995 Hyogoken-Nambu earthquake. Soils and Foundations 38, 163–177.
Tomasello, G., Porcino, D.D., 2022. Influence of sloping ground conditions on cyclic liquefaction behavior of sand under simple shear loading. Soil Dynamics and Earthquake Engineering 163 107516.
Tonni, L., Gottardi, G., Amoroso, V.G., Aversa, S., 2015. Interpreting the deformation phenomena triggered by the 2012 Emilia seismic sequence on the Canale Diversivo di Burana banks. Italian Geotechnical Journal 2, 28–58 (in Italian).
Towhata, I., Orense, R.P., Toyota, H., 1999. Mathematical principles in prediction of lateral ground displacement induced by seismic liquefaction. Soils and Foundations 39 (2), 1–19.
Towhata, I., Maruyama, S., Kasuda, K.I., Koseki, J., Wakamatsu, K., Kiku, H., et al., 2014. Liquefaction in the Kanto region during the

2011 off the pacific coast of Tohoku earthquake. Soils and Foundations 54 (4), 859–873.
Uzuoka, R., Yashima, A., Kawakami, T., Konrad, J.M., 1998. Fluid dynamics based prediction of liquefaction induced lateral spreading. Computers and Geotechnics 22 (3–4), 243–282.
Vannucchi, G., Crespellani, T., Facciorusso, J., Ghinelli, A., Madiai, C., Puliti, A., Renzi, S., 2012. Soil liquefaction phenomena observed in recent seismic events in Emilia-Romagna Region. Italy. International Journal of Earthquake Engineering 2 (3).
Yang, J., Sze, H.Y., 2011a. Cyclic behaviour and resistance of saturated sand under non-symmetrical loading conditions. Géotechnique 61 (1), 59–73.
Yang, J., Sze, H.Y., 2011b. Cyclic strength of sand under sustained shear stress. Journal of Geotechnical and Geoenvironmental Engineering 137 (12), 1275–1285.
Zhou, E.Q., Lv, C., Wang, Z.H., Chen, G.X., 2014. Fluid Characteristic of Saturated Sands under Cyclic Loading. In Advances in Soil Dynamics and Foundation Engineering, pp. 178–186.